DOI: 10.14264/uql.2020.604

# Analysis of two-phase flows in plunge pools of nappe jets

J. M. Carrillo[1], F. Marco[1], L. G. Castillo[1] and J. T. García[1]
[1]Escuela Técnica superior de Ingeniería de Caminos, Canales y Puertos e Ingeniería de Minas
[1]Universidad Politécnica de Cartagena
Cartagena, Spain
E-mail: jose.carrillo@upct.es

*ABSTRACT*

*This study presents an experimental work to analyse the submerged hydraulic jump generated downstream of overflow nappe impinging jets. The overflow structure consists in a sharp-crested weir located at an elevation of 2.20 m from the bottom of the plunge pool. To advance in the understanding of the phenomenon, the velocity field and air entrainment rate were measured with optical fiber and modified Pitot tube in different sections of the submerged hydraulic jump. For the Pitot tube, GE Druck model UNIK 5000 pressure transducers have been used to measure the static and the dynamic pressures. The output signal of both ports was scanned at 20 Hz for 60 s. The optical fiber measurements were carried out with a RBI-instrumentation equipment. Each point was measured during 90 s in the same locations registered by the Pitot tube. The study is focused on the analysis of the local air entrainment concentration, bubble frequency, Sauter mean bubble diameter, mean velocity near the bottom, and free surface undulation pattern.*

***Keywords:*** *air-water flow, submerged hydraulic jump, falling jet, optical fiber probe, overtopping.*

## 1. INTRODUCTION

In recent years, the improvement in time-series knowledge and the recent change in dam and reservoir safety regulations have generated the re-evaluation of the spillways capacity and their operation scenarios for large dams around the world. The studies have raised that the current capacity of many spillways may be insufficient, increasing the possibility of overflow during extreme events. The overtopping creates new loading scenarios for the dams and raises questions about erosion and scour at the dam toe (Wahl et al. 2008).

In general, choosing the type of plunge pool is a technical-economic decision between a deep and unprotected stilling basin and a shallow stilling basin with lining. For a safe operation, it is necessary to know the magnitude and frequency of the dynamic pressure at the bottom of the plunge pool. The required water cushion depth depends on the characteristics of the impingement jet so that the bottom may resist the scour downstream of the dam (Annandale 2006).

The characteristics of free turbulent jets entering into plunge pools have been analyzed by several authors (e.g. Albertson et al. 1950, Beltaos and Rajaratnam 1973, Ervine and Falvey 1987, Ervine et al. 1997, Chanson et al. 2004, Bertola et al. 2018, Xu et al. 2018).

Having a better knowledge of the flow pattern in the plunge pool is important for the designers as it may affect their projects. The effects of entrapped air in the submerged hydraulic jump may be essential for hydraulic structure safety operations.

The hydraulic jump is a sudden transition from a supercritical flow regime to a subcritical regime with high energy dissipation. It may be used as an energy dissipater whose efficiency is directly linked to the strength of the jump. The hydraulic jump is characterized by the development of large-scale turbulence, surface waves and spray, energy dissipation and air entrainment. The air is entrained at the jump toe into a free shear layer, characterized by intensive turbulence production, predominantly in vortices with axes perpendicular to the flow direction.

A better understanding of mixing, diffusion, transfer processes and air/water gas exchanges is strongly dependent on the ability to investigate these two-phase flows (Murzyn 2010). Fig. 1 shows a schematic representation of the submerged hydraulic jump in a plunge pool.

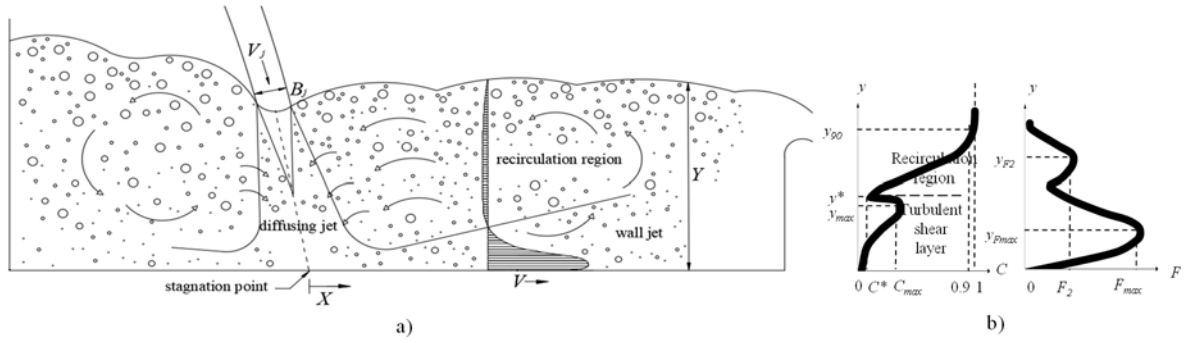


Figure 1. a) Schematic representation of the submerged hydraulic jump in a plunge pool; b) Scheme of distributions of air-water flow properties observed in free hydraulic jumps (left: void fraction; right: bubble frequency)

Based on air concentration or void fraction vertical profiles, several studies (Chanson 1995b, Murzyn and Chanson 2007, Murzyn 2010) identify two regions in free hydraulic jumps: an air-water shear layer in the lower part of the flow with high air content and smaller bubble sizes (millimeters typically), and a recirculating area located in the upper part of the flow. This second region is characterized by strong unsteady recirculation, with small and large size bubbles, and air-water packets. A foam structure layer may be considered near the free-surface. The boundary between these two regions is found at a certain height ($y^*$) above the bottom and it is well defined from the void fraction measurements.

To date, information regarding the behavior of air-water flows in the plunge pool of free-falling jets is scarce (Castillo and Carrillo 2017, Castillo et al. 2017, Carrillo et al. 2019). This work seeks to improve this research field. This study presents an experimental work to analyze the submerged hydraulic jump generated downstream of a sharp-crested weir with the crest located at elevation of 2.20 m from the bottom of the plunge pool. A back-flushing Pitot tube and an optical fiber probe have been used to measure the velocity field and the air entrainment rate, respectively. Mean velocities near the bottom, air entrainment concentration, bubble detection frequency, Sauter mean diameter and free surface undulation pattern have been analyzed in different cross-sections located downstream of the impingement point of free falling jet.

## 2. MATERIALS AND METHODS

### 2.1. Experimental Setup

The experimental device is located in the Hydraulic Laboratory - Universidad Politécnica de Cartagena (Spain). It has been designed for the study of turbulent jets and energy dissipation in overflow weirs. The facility has been modified from that used by Carrillo (2014) to increase the range of flows tested, to improve the energy dissipation in the inlet channel before the weir, and to enhance the falling heights measurements. The current installation allows the analysis of flows between 10 and 200 l/s and falling heights between 2.20 and 3.50 m.

The infrastructure consists of a mobile device located in the upper part and a fixed basin located in the lower part. The mobile mechanism allows stabilizing the flow, through serval energy dissipation systems. Before the sharp-crested weir there is an inlet channel with 4 m length and 1.00 m wide. At the end of this channel, a rectangular sharp-crested weir with a width of 0.85 m and weir height of 0.325 m was installed. The fixed stilling basin, built in methacrylate, allows different depths of water cushions, from direct impact to depths of 1.00 m. Its dimensions are 1.05 m wide, 3.00 m long and 1.60 m high.

In this study, the weir crest elevation was located 2.20 m from the bottom of the plunge pool. A modified Pitot tube and an optical fiber probe were used to measure the velocity field and the air entrainment rate. A trolley was used to support and locate the equipment in the desired position. The accuracy of the location was obtained by rules in the longitudinal, transverse and vertical translations (accuracy ±0.001 m).

The equipment was mounted on a trolley that enables longitudinal and transverse translations. The optical probe and the Pitot tube were positioned in the centerline of the basin. Different cross sections located downstream of

the stagnation point of the impingement jet were analyzed, with distances of 0.10 m between them. In each section, the vertical profiles were measured.

Two different submerged hydraulic jumps were analyzed in the stilling basin: $q = 0.085$ m$^3$/s/m, $Y = 0.34$ m, and $q = 0.099$ m$^3$/s/m, $Y = 0.30$ m, being $q$ the specific flow and $Y$ the water depth at the end of the plunge pool.

To minimize the scale effects on Froude $F_r$ similarity scale models of hydraulic jumps and vertical plunging jets, Chanson (2009) and Heller (2011) considered that the Reynolds $R_e$ and Weber $W_e$ numbers should be larger than $10^5$ and $10^3$, respectively. Following Castillo et al. (2015), the Reynolds $R_e$ and Weber $W_e$ numbers may be obtained at issuance conditions of the nappe flow case, located at a vertical distance $h$ downstream of the weir crest: $R_e = 139{,}201$, $W_e = 6{,}454$ for $q = 0.085$ m$^3$/s/m; $R_e = 119{,}315$, $W_e = 5{,}256$ for $q = 0.099$ m$^3$/s/m. These values accomplish the recommendations for $R_e$ and $W_e$ numbers. However, as the air bubble size is not correctly scalable, phenomena including air flow have to be scaled with special caution (Chanson, 2009).

## 2.2. Optical Fiber Probe

An optical fiber equipment from RBI-Instruments was used to obtain the local void fraction. The optical probe sensitive area consists in a Descartes prism; depending on the refraction index of the medium in contact with the prism and on the angle of incidence of the ray of light, this ray is either reflected or diffracted by the prism. The signal is converted into voltage in an optoelectronic module. Thus, optical fiber equipment allows estimating the phase change between air and water (RBI-Instruments 2012). The rise and fall of the signal detected are, respectively, the arrival and departure of the change phase at the sensor tip. The threshold values were set at 0V (liquid) and 5 V (air).

According to Murzyn et al. (2005), in a slow moving flow the smallest detectable bubble may be of the order of the optical fiber diameter (40 μm). However, at higher velocities the limiting size becomes a function of the signal settling time (1 μs).

The local void fraction ($C_{air}$) may be defined as the ratio between the total time the probe is in air ($\Sigma_{tGi}$) and the time duration $t$ of the sample. This equipment allows to measure air-water flows with velocities up to 20 m/s. The relative uncertainty of the void fraction is estimated at approximately 15% of the measured value, and the sensitivity to a threshold variation of 1% is less than 1% (Stutz and Reboud 1997a, 1997b).

A source of error in estimating the presence of air in the flow is due to the statistical count of the number of air bubbles in contact with the tips of the probe (Stutz 1996). Therefore, a short duration of the measurement would contribute to a lower results' accuracy. Boes and Hager (2003) carried out experiments with 4000 air bubbles and samplings of 30 s. The authors considered that the accuracy of the void fraction and velocity measurements is related to the variation of the phase, air/water variation or the inverse, rather than the sample duration $t$. To evaluate the minimum duration of the measurements, André et al. (2005) analyzed the time required to stabilize the mean value during the measurement and that the quasi-stationary values were statistically representative of the void fraction. Based on the sensitivity study of the probe behavior, the authors recommend a 60 s sampling sequence as a good compromise between precision and duration of the experiments. To err on the side of caution, this study has considered a sample sequence of 90 s. In addition, a relative uncertainty of less than 1% of the evolution of the void fraction has been verified with this sample duration in this type of tests. Further details may be found in Carrillo et al. (2018, 2019).

With those considerations, the two-phase flow characteristics were measured in different cross-sections spaced 0.10 m downstream of the stagnation point of the plunge pool with the probe perpendicular to the bottom. These results allowed to obtain the local void fraction, and the water depths in where the local void fraction was 20 and 90% ($y_{20}$ and $y_{90}$, respectively), among other parameters.

## 2.3. Back-Flushing Pitot Tube

A Pitot tube was used for measuring the velocity profiles of the plunge pool in the same locations measured with the optical fiber equipment. The Pitot tube measures the pressure difference between the dynamic pressure at the tip of the tube (through a 2.3 mm hole), and the static pressure, measured by a ring of ports located in the circumference of the Pitot tube. The external diameter of the Pitot tube is 12 mm. Pressure transducers GE

Druck model UNIK 5000 were used to record the pressures variations. These sensors have a measuring range between -200 and +800 mbar and a full scale accuracy of ±0.04%. After carrying out a static calibration, the pressure accuracy of the transducers was ±0.01 m. The pressure transducers were located at the bottom of the plunge pool. The output signal of both ports was scanned at 20 Hz for 90 s (1800 data).

To avoid air entered into the pneumatic system of the Pitot tube during the tests, continuous back-flushing was forced, by means of a constant head source which fed both the static pressure and the dynamic pressure of the Pitot tube (Matos and Frizell 2000, Matos et al. 2002, Bombardelli et al. 2011). The back-flushing flow was controlled by needle valves. To reduce the perturbation of the measurements, the back-flushing flow rate to each port was limited to almost zero.

Wood (1983) determined the time-averaged velocity from the measured pressure of the Pitot tube in air-water flows as:

$$V = \sqrt{\frac{2g\Delta P}{\rho_w(1-\lambda C_{air})}} \tag{1}$$

where $V$ is the velocity, $g$ gravity acceleration, $\Delta P$ the difference between the total pressure head and the static pressure head, $\rho_w$ the density of water, $C_{air}$ the local void fraction (volume of air per total volume), and $\lambda$ the tapping coefficient which accounts for the non-homogeneous behavior of the air-water flow approaching the stagnation point of the Pitot tube.

The recirculating region may affect the measurements of the Pitot tube (Matos and Frizell 2000, Matos et al. 2002). For this reason, local velocities were limited to the wall jet near the bottom region.

## 3. RESULTS AND DISCUSSION

### 3.1. Void Fraction in the Plunge Pool

According to Wood (1991), void fraction and their corresponding air concentration is one of the key parameters to be analyzed in the submerged hydraulic jump generated in the basin. The effects of entrained air may be essential for the safety operation of hydraulic structures.

Optical fiber methodology was used in the dissipation basin to obtain the void fraction profiles downstream of the impingement point of the rectangular free-falling jet. Different cross sections spaced every $X = 0.10$ m ($X$ = horizontal distance from the stagnation point) were analyzed. In each cross section, more than 50 points were measured. Fig. 2 shows the void fraction profiles ($C_{air} = \Sigma_{tGi}/t$) of the two flows analyzed in the laboratory. The vertical axis has been normalized, considering the $y_{90}$ value (distance at which $C_{air} = 90\%$).

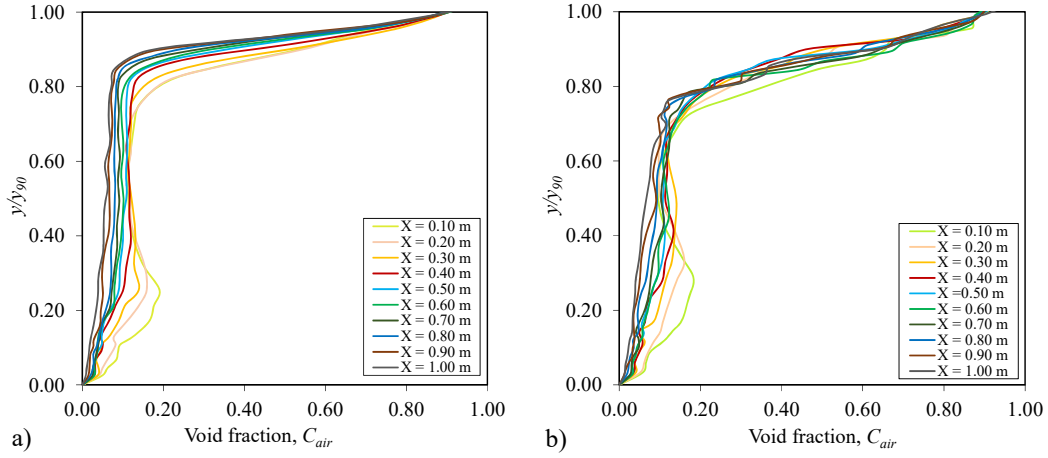


Figure 2. Void fraction profiles downstream of the stagnation point: a) $q = 0.085$ m$^3$/s/m, $Y = 0.34$ m; b) $q = 0.099$ m$^3$/s/m, $Y = 0.30$ m

Near the bottom ($0.15 < y/y_{90} < 0.35$), the largest values of void fraction were obtained close to the stagnation point of the rectangular jet, reaching values of around 15-20% in both submerged hydraulic jumps. As the flow moves downstream from the jet's impact zone, the void fraction detected by the probe tends to decrease. The profiles located at distances greater than $X = 0.60$ m from the stagnation point present void fractions lower than 10%, reaching values around 7-8% in the profile located at $X = 1.00$ m (for $y/y_{90} < 0.70$-$0.80$). For $y/y_{90} > 0.80$, the air entrainment values increase rapidly. This may indicate the layer of the unsteady flow depth generated by the surface undulation at a given location.

Fig. 3 shows the data in a dimensionless way as a function of the average concentration in the vertical. The mean void fraction ($C_{mean}$) in the cross-section is defined as:

$$C_{mean} = \frac{1}{Y_{90}} \int_0^{y90} C_{air}\, dy \tag{2}$$

In general, both specific flows show the same trend in each sub-class. In Fig. 3 the theoretical law for the diffusion of air bubbles in air-water emulsion developed by Chanson (1995a) for free-surface aeration by turbulence in uniform equilibrium flow has been also represented for several mean void fractions.

$$C_{air} = 1 - tanh^2\left(K' - \frac{y'}{2D'}\right) \tag{3}$$

where $K'$ is an integration constant, $D'$ is a dimensionless turbulent diffusivity (assuming a homogeneous turbulence) and $y' = y/y_{90}$.

Although Eq. (3) was not developed for submerged hydraulic jumps, it may provide a point of reference for comparison. The data of $C_{mean}$ between 0.15 and 0.30 tend to fall between the theoretical laws of 0.10 and 0.20 mean void fractions for $y/y_{90} > 0.60$.

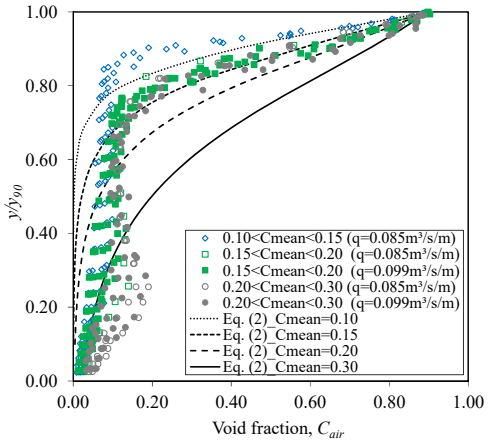


Figure 3. Comparison of void fraction profiles as a function of the mean void fraction ($C_{mean}$)

## 3.2. Free Surface Undulation Pattern

To analyze the free surface undulation in the plunge pool, the equivalent water height (defined as the equivalent water depth that would be in the absence of aeration) may be obtained as:

$$h_{eq} = (1 - C_{mean}) y_{90} \tag{4}$$

Fig. 4 shows the depths in each cross section related with the void fraction of 20 and 90% ($y_{20}$ and $y_{90}$, respectively), and the equivalent water depth ($h_{eq}$) for the two studied flows as a function of $Y$ (value $y_{90}$ of section $X = 1.0$ m). In both flows, the $h_{eq}$ and $y_{20}$ values have very similar results. The distance between $y_{20}$ and $y_{90}$ tends to decrease as the flow moves away from the stagnation point. This means that there is a decrease in the mean void fraction along the dissipation bowl.

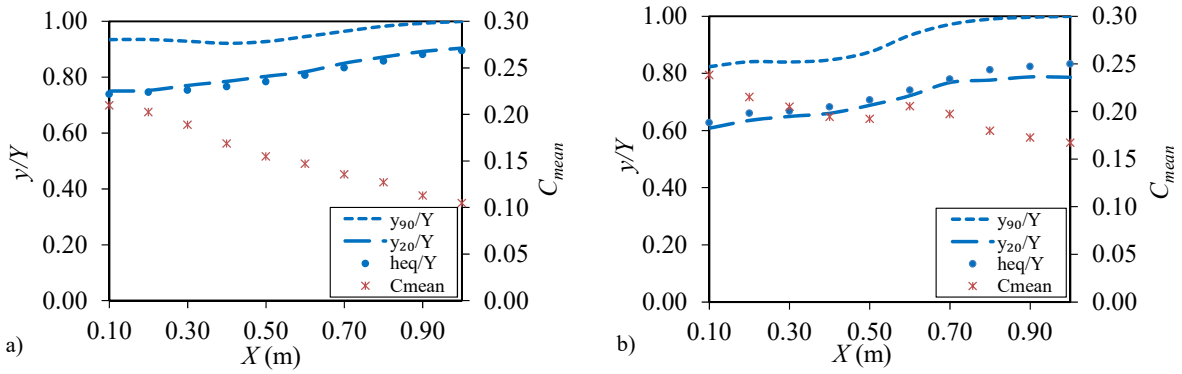


Figure 4. Variation of the free surface undulation pattern and mean void fraction: a) $q$ = 0.085 m$^3$/s/m, $Y$ = 0.34 m; b) $q$ = 0.099 m$^3$/s/m, $Y$ = 0.30 m

## 3.3. Bubble Frequency

Bubble detection frequency has been analyzed by different authors in free hydraulic jumps (e.g., Murzyn et al. 2005, Murzyn and Chanson 2007). However, there are few references to submerged hydraulic jumps downstream of nappe flows (Castillo et al. 2017, Carrillo et al. 2018, 2019).

Fig. 5a provides a comparison of the two flows by doing dimensionless the horizontal distance with the impingement jet thickness $B_j$. The impingement jet thickness formula is obtained as (Castillo et al. 2015):

$$B_j = B_g + 2\xi = \frac{q}{\sqrt{2gH}} + 4\varphi\sqrt{h}\left(\sqrt{2H} - 2\sqrt{h}\right) \quad (5)$$

where $B_g$ is the thickness due to gravitational effect, $x$ the lateral jet spread distance due to the turbulence effect, $q$ the specific flow, $H$ the fall height, and $h$ is the energy head at the weir crest. $\varphi = K_\varphi \cdot T_u$, with $T_u$ being the turbulence intensity and $K_\varphi$ = 1.24 for nappe flow case.

Fig. 5a shows the bubble frequency detected by the optical probe. Both flows show the same trend in their behavior. In most of the profiles, the highest values are obtained in the vicinity of the bottom. In the profiles located in ratios $X/B_j$ < 10 downstream of the stagnation point, maximum values of around 130-140 Hz were obtained. The maximum values tend to decrease as the flow moves away from the stagnation point. In the profile located at $X/B_j$ > 30, the frequency tends to be around 20-30-40 Hz ($q$ = 0.085 m$^3$/s/m, $Y$ = 0.34 m) and 40-50 Hz ($q$ = 0.099 m$^3$/s/m, $Y$ = 0.30 m) for almost the entire depth (0.20 < $y/y_{90}$ < 0.80).

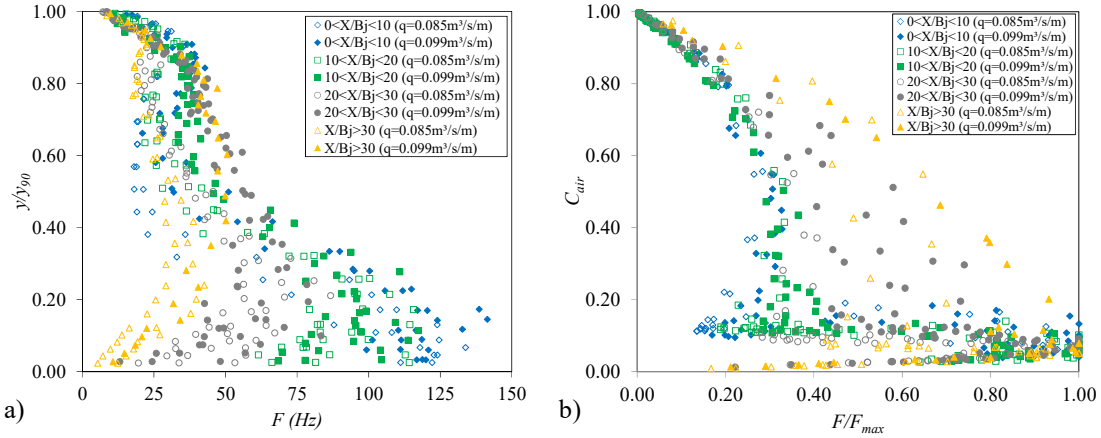


Figure 5. a) Bubble detection frequency profiles downstream of the stagnation point. b) Normalized frequency profiles with respect to the maximum frequency

The impingement Froude numbers were estimated to be around 11.62 ($q$ = 0.085 m$^3$/s/m, $Y$ = 0.34 m) and 11.11 ($q$ = 0.099 m$^3$/s/m, $Y$ = 0.30 m). The values recorded were similar to the results obtained by Murzyn and

Chanson (2007) in free hydraulic jumps, who measured maximum frequencies of around 120 Hz with Froude number of 8.30, and relatively larger than those of Murzyn et al. (2005), who obtained maximum frequencies of around 85 Hz in free hydraulic jumps with a Froude number of 4.82.

The frequency profiles may be compared if they are normalized with the maximum frequency $F_{max}$ (see Fig. 5b). In both flows, two different grouping are observed. The higher frequencies are obtained for low concentration values ($C_{air}$ < 0.10). For $X/B_j$ < 20 the $F/F_{max}$ values are around 0.30 for $C_{air}$ between 0.20 and 0.80. As the flow moves from the impingement point, and the detection frequency tends to decrease, the $F/F_{max}$ values are more scattered. Near the free surface ($C_{air}$ > 0.80), the $F/F_{max}$ ratio tends to rapidly decrease.

## 3.4. Distribution of Velocities in the Dissipation Basin

Mean velocity measurements were obtained with the modified Pitot tube corrected by the local void faction with Eq. (1). The laboratory equipment allows to analyze the wall jet. Near the bottom, the streamlines are parallel and the laboratory equipment seems to be accurate. Outside the wall jet, the streamlines are not parallel to the bottom and the laboratory measurements may be affected by the velocity vector angle (Matos and Frizell 2000, Matos et al. 2002). For that reason, laboratory velocities were not recorded in the roller region.

The velocity profiles in the forward flow of hydraulic jumps can be compared if they are normalized with a velocity scale equal to the maximum velocity $V_{max}$ at any section, and with a length scale $\delta_l$ equal to the vertical distance $y$ from the bottom where the local velocity $V = V_{max}/2$, and the velocity gradient is negative (Rajaratnam 1965).

The maximum velocity $V_{max}$ and the length scale $\delta_l$ were calculated in each cross section of the submerged hydraulic jump. The maximum mean velocity was 1.58 m/s for $q$ = 0.085 m$^3$/s/m and for 2.19 m/s for $q$ = 0.099 m$^3$/s/m. Fig. 6 shows the non-dimensional velocity profiles in cross sections located from 0.10 to 1.00 m downstream of the stagnation point. The highest velocities have been registered in the vicinity of the bottom and tend to decrease as the flow moves to the free surface. The results obtained are also in agreement with non-dimensional velocity distribution formulae obtained by several authors (Table 1).

Table 1. Formulae of the velocity distribution in wall jets and hydraulic jumps

| Author | Formula | Investigation |
|---|---|---|
| Görtler (1942), cited by Liu et al. (1998) | $\frac{V_x}{V_{max}} = 1 - tanh^2\left(0.881\frac{y}{\delta_l}\right)$ | Plane free jet |
| Rajaratnam (1976) | $\frac{V_x}{V_{max}} = e^{-0.693\left(\frac{y}{\delta_l}\right)^2}$ | Plane turbulent free jet |
| Lin et al. (2012) | $\frac{V_x}{V_{max}} = 2.3\left(\frac{y}{\delta_l}\right)^{0.42}\left(1 - erf\left(0.886\frac{y}{\delta_l}\right)\right)$ | Free jump |
| De Dios et al. (2017) | $\frac{V_x}{V_{max}} = 2.0\left(\frac{y}{\delta_l}\right)^{1/7}\left(1 - erf\left(0.55\frac{y}{\delta_l}\right)\right) - 0.39$ | Submerged hydraulic |
| Castillo et al. (2017) | $\frac{V_x}{V_{max}} = 1.48\left(\frac{y}{\delta_l}\right)^{1/7}\left(1 - erf\left(0.66\frac{y}{\delta_l}\right)\right)$ | Submerged hydraulic jump |

where $erf(u) = \frac{2}{\sqrt{\pi}}\int_0^u e^{-t^2}dt$

## 3.5. Mean Bubble Size

Several researchers have observed that the bubble shape may be related with the size of the bubbles (Harmathy 1960). Small bubbles tend to be of spherical or slightly ellipsoidal shape while larger bubbles have a more definite ellipsoidal shape, becoming more distorted and less definite with increasing size.

Assuming the hypothesis that bubbles are spherical, equally distributed in time and that their movement is one-directional, the size of the bubbles detected by the optical fiber equipment may be characterized by the Sauter mean bubble diameter, $D_{sm}$ (Clift et al. 1978, RBI-Instrumentation 2012). This is the diameter of the bubbles

whose volume/surface ratio is the same as that calculated for all the bubbles detected during the test. The Sauter mean diameter can be calculated as:

$$D_{sm} = \frac{3C_{air}V}{2F} \tag{6}$$

where $C_{air}$ is the void fraction, $V$ the mean velocity of the bubbles, and $F$ the bubble detection frequency.

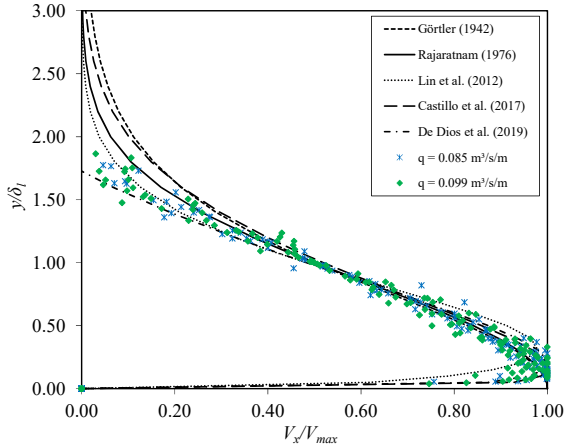


Figure 6. Profiles of horizontal mean velocity in different sections of the plunge pool

The bubble size distributions may be characterized in terms of the bubble chord length, which is obtained as the time of a bubble spent on the phase-detection probe tip multiplied by the local velocity. Assuming the velocity field obtained in the previous section, Fig. 7 shows the probability to find each bubble size in three different locations of the wall jet, obtained in three different cross sections ($X$ = 0.10 m, $X$ = 0.50 m and $X$ = 0.90 m). The probability distribution function (PDF) tends to decrease as the bubble chord size increases and as the flow moves away from the impact zone. The bubble chord length between 0 and 0.2 mm seems to have a higher probability of occurrence.

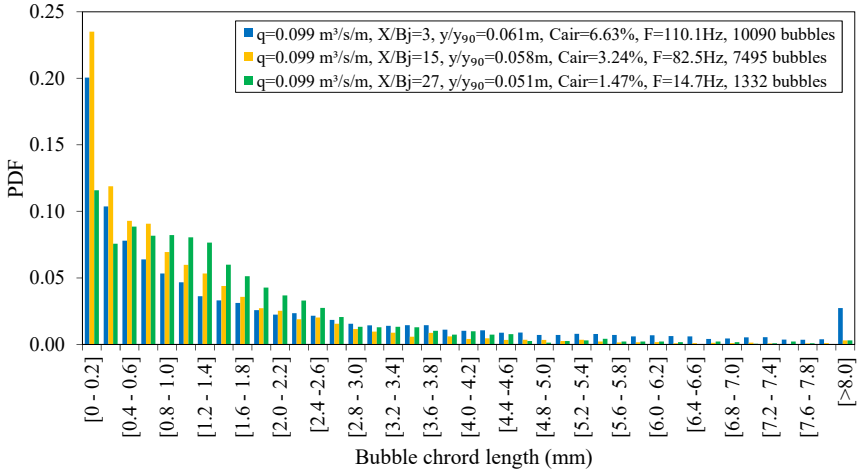


Figure 7. Probability distribution function (PDF) of the bubbles chord length downstream of the stagnation point for a flow rate of $q$ = 0.099 m$^3$/s/m, $Y$ = 0.30 m

## 4. CONCLUSIONS

To observe and to predict two-phase flows in hydraulic structures is very complicated because of the undiluted nature of the flow.

In this work, the characteristics of the air-water flow produced downstream of an overflow weir have been analyses. Optical fiber and back-flushing Pitot tube equipment were mainly used in the quasi unidirectional flow region of the submerged hydraulic jump to estimate the void fraction and the velocity fields in the plunge pool.

Near the bottom ($0.15 < y/y_{90} < 0.40$), the greater values of void fraction were obtained close to the stagnation point of the rectangular jet. The air void fraction tends to decrease as the flow moves downstream from the impact zone of the nappe jet. In an intermediate zone ($0.40 < y/y_{90} < 0.80$), the values remain around a constant value in the profile. Near the free surface ($y/y_{90} > 0.80$), the void fraction values increase rapidly in all the cross sections due to the surface undulation.

The larger values of bubble frequency were obtained close to the stagnation point of the rectangular jet and near the bottom of the plunge pool ($y/y_{90} < 0.25$), with maximum values around 130-140 Hz. The bubble frequency tends to decrease as the flow moves downstream from the impingement point.

A higher probability distribution function has been found for values of bubble chord length between 0 and 0.2 mm. This probability tends to decrease as the chord length size increases. At $X = 0.90$ m from the stagnation point, the PDF shows similar chord length values between 0.10 and 1.30 mm.

In general, the characteristics of the air distribution (void fraction, bubble frequency and Sauter mean bubble diameter) are similar to those observed in free hydraulic jumps with different Froude numbers. The velocities obtained near the bottom are also in agreement with non-dimensional velocity distribution formulae obtained by several authors. This allows us to consider that our results may describe the submerged hydraulic jump downstream of a nappe flow case.

## 5. ACKNOWLEDGMENTS

The researchers express their gratitude for the financial aid received from the Ministerio de Ciencia, Innovación y Universidades and the Fondo Europeo de Desarrollo Regional (FEDER), through the Project "La aireación del flujo en el vertido en lámina libre por coronación de presas a nivel de prototipo y su efecto en cuencos de disipación de energía", Reference (RTI2018-095199-B-I00).

The second author would like to thank the Ministerio de Educación, Cultura y Deporte for the financial aid received from the University Teacher Training Grant (FPU), reference number FPU16 / 05658.

## 6. REFERENCES

Albertson, M.L., Dai, Y.B., Jenson, R.A., and Rouse, H. (1950). Diffusion of submerged jets. *Procs. ASCE*, 74.
André, S., Boillat, J.L., and Schleiss, A.J. (2005). Discussion of 'Two-phase flow characteristics of stepped spillways' by Robert M. Boes and Willi H. Hager. *Journal of Hydraulic Engineering*, 131(5), 423–427.
Annandale, G.W. (2006). Scour Technology. Mechanics and Engineering Practice. McGraw-Hill, New York.
Beltaos, S., and Rajaratnam, N. (1973). Plane turbulent impinging jets. *Journal of Hydraulic Research*, 11(1), 29-59.
Bertola, N., Wang, H., and Chanson, H. (2018). A physical study of air–water flow in planar plunging water jet with large inflow distance. *International Journal of Multiphase Flow*, 100, 155-171.
Boes, R., and Hager, W.H. (2003). Two-phase flow characteristics of stepped spillways. *Journal of Hydraulic Engineering*, 129(9), 661–670.
Bombardelli, F.A, Meireles, I., and Matos, J. (2011). Laboratory measurements and multi-block numerical simulations of the mean flow and turbulence in the non-aerated skimming flow region of steep stepped spillways. *Environ Fluid Mech*, 11, 263–288.
Carrillo, J.M. (2014). Metodología numérica y experimental para el diseño de los cuencos de disipación en el sobrevertido de presas de fábrica. PhD Thesis. Universidad Politécnica de Cartagena, Spain (in Spanish).
Carrillo, J.M., Castillo, L.G., Marco, F., and García, J.T. (2018). Characterization of two-phase flows in plunge pools. *Proc., 7th IAHR International Symposium on Hydraulic Structures*, Aachen, Germany, 15-18 May. doi: 10.15142/T3JM1W (978-0-692-13277-7).
Carrillo, J.M., Castillo, L.G., Marco, F., and García, J.T. (2019). Experimental and numerical analysis of two-phase flows in plunge pools. *Journal of Hydraulic Engineering*, ASCE, doi: 10.1061/(ASCE)HY.1943-7900.0001763.
Castillo, L.G., and Carrillo, J.M. (2017). Comparison of methods to estimate the scour downstream of a ski jump. *International Journal of Multiphase Flow*, 92, 171-180.
Castillo, L.G., Carrillo, J.M., and Blázquez, A. (2015). Plunge pool mean dynamic pressures: a temporal analysis in nappe flow case. *Journal of Hydraulic Research*, 53(1), 101–118.

Castillo, L.G., Carrillo, J.M., and Bombardelli, F.A. (2017). Distribution of mean flow and turbulence statistics in plunge pools. *Journal of Hydroinformatics*, 19(2), 173-190.
Chanson, H. (1995a). Air bubble entrainment in free-surface turbulent flow. Report CH46/95, University of Queensland.
Chanson, H. (1995b). Air entrainment in two dimensional turbulent shear flows with partially-developed inflow conditions, *International Journal of Multiphase Flow,* 21(6): 1107-1121.
Chanson, H. (2009). Turbulent air-water flows in hydraulic structures: dynamic similarity and scale effects. *Environ Fluid Mech*, 9, 125-142.
Chanson, H., and Brattberg, T. (2000). Experimental study of the air–water shear flow in a hydraulic jump. *International Journal of Multiphase Flow*, 26(4), 583–607.
Chanson, H., Aoki, S., and Hoque, A. (2004). Physical modelling and similitude of air bubble entrainment at vertical circular plunging jets. *Chemical Engineering Science*, 59, 747-758.
Clift, R., Grace, J.R., and Weber, M.E. (1978). Bubbles, drops and particles. Academic Press, New York.
De Dios, M., Bombardelli, F.A., García, C.M., Liscia, S.O., Lopardo, R.A., and Parravicini, J.A. (2017). Experimental characterization of three-dimensional flow vertical structures in submerged hydraulic jumps. *Journal of Hydro-environment Research*,15, 1-12.
Ervine D.A. and Falvey, H.T. (1987). Behavior of turbulent eater jets in the atmosphere and in plunge pools. Proceedings of the Institutions of Civil Engineers, 83 (2), 295-314.
Ervine D.A., Falvey, H.T. and Withers W. (1997). Pressure fluctuations on plunge pool floors. *Journal of Hydraulic Research*, 35(2), 257–279.
Harmathy, T.Z. (1960). Velocity of Large Drops and Bubbles in Media of Infinite or Restricted Extent. *AIChE Journal*, 6, 281-288.
Heller, V. (2011). Scale effects in physical hydraulic engineering models. *Journal of Hydraulic Research*, 49(3), 293-306.
Lin, C., Hsieh, S.-C., Lin, I.-J., Chang, K.-A., and Raikar, R. V. (2012). Flow property and self-similarity in steady hydraulic jumps. *J. Exp. Fluids,* 53, 1591–1616.
Liu, P., Gao, J., and Li, Y. (1998). Experimental investigation of submerged impinging jets in a plunge pool downstream of large dams. *Sci. China: Technological Sciences*, 41(4), 357–365.
Matos, J., Frizell, K.H., André, S., and Frizell, K.W. (2002). On the performance of velocity measurement techniques in air-water flows. *Proceedings of the Hydraulic Measurements and Experimental Methods Conference*, EWRI/ASCE & IAHR, Estes Park, USA.
Matos, J., and Frizell, K.H. (2000). Air concentration and velocity measurements on self-aerated flow down stepped chutes. *Proc., 2000 Joint Conf. on Water Resources Engineering and Water Resources Planning & Management*, ASCE, Minneapolis, USA.
Murzyn, F. (2010). Assessment of different experimental techniques to investigate the hydraulic jump: do they lead to the same results? *Proc., 3rd International Junior Researcher and Engineer Workshop on Hydraulic Structures*, May 02-04, Edinburg, UK, 3-36.
Murzyn, F., and Chanson, H. (2007). Free surface, bubbly flow and turbulence measurements in hydraulic jumps, Report N°CH63/07, Division of Civil Engineering, The University of Queensland, Brisbane, Australia.
Murzyn, F., Mouaze, D., and Chaplin, J.R. (2005). Optical fibre probe measurements of bubble flow in hydraulic jumps. *International Journal of Multiphase Flow*, 31, 141-154.
Rajaratnam, N. (1965). The hydraulic jump as wall jet. *Proc. ASCE J. Hydraul. Div. 91 (HY5)*, 107–132.
Rajaratnam, N. (1976). Turbulent Jets. Elsevier Scientific, Development in Water Science, 5, New York, USA.
RBI-Instrumentation (2012). ISO Software user's guide.
Stutz, B. (1996). Analyse de la structure diphasique et instationnaire de poches de cavitation. PhD Thesis, Institut National Polytechnique de Grenoble, France (in French).
Stutz, B., and Reboud, J.L. (1997a). Experiment on unsteady cavitation. *Experiments in Fluids*, 22, 191–198.
Stutz, B., and Reboud, J.L. (1997b). Two-phase flow structure of sheet cavitation. *Physics of Fluids*, 9(12), 3678–3686.
Wahl, T.L., Frizell, K.H., and Cohen, E.A. (2008). Computing the trajectory of free jets. *Journal of Hydraulic Engineering*, 134(2), 256–260.
Wood, I. R. (1983). Uniform region of self-aerated flow. *Journal of Hydraulic Div*., ASCE, 109(3), 447–461.
Wood I. R. (1991). Air entrainment in free-surface flows. IAHR. ISBN: 90-6191-994-0.
Xu W., Chen C. and Wei W. (2018). Experimental Study on the Air Concentration Distribution of Aerated Jet Flows in a Plunge Pool. *Water* 2018, 10, 1779.